

Proposal for the generation of continuous-wave vacuum ultraviolet laser light for Th-229 isomer precision spectroscopy

Qi Xiao,¹ Gleb Penyazkov,¹ Ruihan Yu,¹ Beichen Huang,¹ Jiatong Li,¹ Juanlang Shi,¹ Yanmei Yu,^{2,3,*} Yuxiang Mo,^{1,†} and Shiqian Ding^{1,‡}

¹*State Key Laboratory of Low Dimensional Quantum Physics,
Department of Physics, Tsinghua University, Beijing 100084, China*

²*Beijing National Laboratory for Condensed Matter Physics,
Institute of Physics, Chinese Academy of Sciences, Beijing, 100190, China*

³*University of Chinese Academy of Sciences, 100049 Beijing, China*

(Dated: June 25, 2024)

We propose to generate continuous-wave vacuum ultraviolet (VUV) laser light at 148.4 nm using four-wave mixing in cadmium vapor for precision spectroscopy of the Th-229 isomer transition. Due to the large transition matrix elements of cadmium, the readily accessible wavelengths for the incident laser beams, and the high coherence of the four-wave mixing process, over 30 μW of VUV power can be generated with a narrow linewidth. This development paves the way for coherently driving the Th-229 isomer transition and developing the nuclear optical clock.

The invention of coherent laser sources has revolutionized the field of atomic and molecular physics. The success of these applications can be attributed to the ability to drive transitions in the electron shell using lasers. Expanding these well-established technologies to manipulate nuclear quantum states holds great promise. However, coherent control of nuclear transitions has been challenging [1–3] due to the significant energy gap between the nuclear transitions and the photon energy of coherent laser radiation. A nuclear transition involves large changes of both Coulomb interaction energy and strong interaction energy that are normally a few 10^5 - 10^6 electron volts. A fortuitous cancellation of the changes of these two terms occurs in the well-known Th-229 isomer transition [4, 5], resulting in a nuclear excited state with the lowest known energy that lies only 8.4 eV above the ground state [6–16]. The corresponding transition falls within the range of typical electronic transitions, and is the only nuclear transition that can be driven using currently available laser sources. This offers a unique opportunity to bridge the fields of atomic and nuclear physics and potentially apply quantum technologies developed over the past few decades to nuclei.

One remarkable frontier is the development of a nuclear optical clock [17, 18]. Due to their much smaller size and multipole moments compared to atoms, nuclei exhibit greater robustness in the frequency of nuclear transitions against perturbing external fields. This characteristic can be employed to alleviate the significant effort required to control ambient fields near an atomic optical clock. The use of the Th-229 isomer transition in a nuclear clock is further motivated by its remarkable sensitivity to temporal variations in fundamental constants, such as the fine-structure constant [4, 19–22], and its application in

the search for ultralight dark matter [23, 24].

Another salient feature of nucleus-based experiments is the doping of a large number of atoms into a solid material while generically keeping the nuclear structure intact [17, 25, 26]. This is in contrast to current atomic-shell-based quantum systems, where valence electrons of suspended atoms in the vacuum play a central role, and doping would eliminate the relevant underlying quantum states. Hosting nuclei with a solid material in the Lamb-Dick regime may substantially reduce the required experimental efforts, particularly the challenging tasks of laser cooling and trapping. Additionally, the ability to control a macroscopic quantity of nuclear systems can largely reduce the interrogation time for precision measurements.

Driven by these compelling prospects [27–29], several methods have been employed to measure the energy of the Th-229 isomer transition [6–16], including indirect γ spectroscopy [9, 12, 13], internal-conversion electron spectroscopy [10, 30], and vacuum ultraviolet (VUV) spectroscopy of radiative fluorescence light [14]. Very recently, laser spectroscopy has been finally achieved by two groups based on thorium-doped VUV-transparent crystals [15, 16], and the transition wavelength is determined to be 148.4 nm. In both experiments, tunable pulsed VUV laser sources are produced by four-wave mixing (FWM) in xenon gas, with durations of several nanoseconds, average powers ranging from 30 to 450 μW , and linewidths of a few GHz. The current spectroscopy uncertainty stands at approximately 3 GHz [15, 16], primarily limited by the broad spectral linewidth associated with the pulsed nature of the VUV laser. The radiative lifetime of the isomer state is measured to be between 2000 and 3000 s [14–16, 22, 31], corresponding to a linewidth of around 60 μHz . This significant linewidth disparity of many orders of magnitude underscores the need for a narrow-line laser for efficient transition driving and precision spectroscopy. A highly coherent frequency comb in the VUV region has been demonstrated via high-order harmonic generation (HHG) from an in-

* ymyu@aphy.iphy.ac.cn

† ymo@mail.tsinghua.edu.cn

‡ dingshq@mail.tsinghua.edu.cn

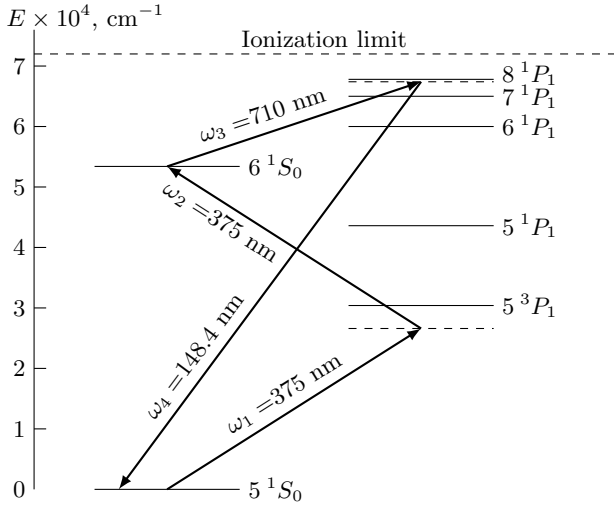


Figure 1. Simplified energy level scheme of neutral Cd. The arrows represent incident lasers with frequencies ω_1 , ω_2 , ω_3 and the generated VUV laser with frequency ω_4 at 148.4 nm.

frared comb [32–34] and is being utilized in Th-229 isomer spectroscopy [28, 35–37]. Although the linewidth of the comb might be as narrow as kHz, a single comb line with a power of only 1 nW contributes to driving the isomer transition [28, 37].

In this work, we propose to generate continuous-wave (CW) laser light at 148.4 nm using four-wave mixing scheme for precision spectroscopy of the Th-229 isomer transition. Cadmium vapor is identified as a promising nonlinear medium capable of producing over 30 μ W of VUV power. The generated VUV laser can achieve a linewidth several orders of magnitude narrower than pulsed FWM sources currently used in isomer spectroscopy [38, 39], and a power more than four orders of magnitude higher than a single comb line in state-of-the-art VUV frequency comb [37]. This approach addresses the challenge posed by the lack of an intense and narrow-linewidth laser near the Th-229 isomer transition [40], enabling coherent driving of nuclear Rabi oscillations.

The FWM process relies on the third-order nonlinear susceptibility, which is the lowest-order nonlinearity observed in an isotropic medium. It has long been employed to generate VUV light [2, 41] that otherwise is challenging to produce for spectroscopy in this wavelength region. The nonlinear process necessitates high incident laser intensities, generally resulting in the generated VUV light being pulsed. A notable exception is the production of CW Lyman- α radiation at 121.6 nm using FWM in mercury vapor [43–45].

For the FWM process considered here, a new wave with the sum frequency of three incident laser beams is generated, $\omega_1 + \omega_2 + \omega_3 \rightarrow \omega_4$, as shown in Fig. 1. For tightly focused incident laser beams with equal confocal parameter b , the FWM output power in the small signal

limit [2] is given by [3]

$$P_4 = \frac{9}{4} \frac{\omega_1 \omega_2 \omega_3 \omega_4}{\pi^2 \epsilon_0^2 c^6} \frac{1}{b^2} \left(\frac{1}{\Delta k_a} \right)^2 |\chi_a^{(3)}|^2 P_1 P_2 P_3 G(bN \Delta k_a), \quad (1)$$

where ω_i is the laser angular frequency, P_i the laser power, N the number density of the nonlinear medium, $\Delta k_a = (k_4 - k_1 - k_2 - k_3)/N$ the wave vector mismatch per atom, $\chi_a^{(3)}$ the third-order nonlinear susceptibility per atom, and $G(bN \Delta k_a)$ the phase matching function.

To understand the FWM process described by Eq. 1, the phase matching function $G(bN \Delta k_a)$ and the calculation of nonlinear susceptibility $\chi_a^{(3)}$ are detailed in the following. The wave vector mismatch Δk_a due to dispersion indicates the momentum mismatch in nonlinear optical processes. In the tight focus limit, where the confocal length of the laser beams b is much smaller than the length of the nonlinear medium L , this mismatch can be compensated by the Gouy phase shift. In this limit, the Gouy phase shift is experienced three times by the incident beams in the Gaussian focus but only once by the frequency-summed generated beam [47]. Thus, the phase matching function $G(bN \Delta k_a)$ is maximized not at $\Delta k_a = 0$ as in the nonlinear optical processes with the collimated beams, but at $bN \Delta k_a = -4$. It is important to note that Δk_a does not depend on the number density of the nonlinear medium (see Supplemental Material [48]) but the frequencies of incident and generated lasers. Therefore, the optimal phase matching condition can be achieved by adjusting b and N accordingly [3].

The calculation of the nonlinear susceptibility $\chi_a^{(3)}$ from the first principles can be found in [49]. We employ the two-photon resonance condition, $\omega_1 + \omega_2 = \omega_{rg}$, to enhance the output VUV power [41], with 6^1S_0 as the resonance state (denoted as r , with ω_{rg} representing its transition frequency to the ground state g). For three linearly polarized incident laser beams, the leading term in $\chi_a^{(3)}$ is [4]

$$\chi_a^{(3)} = \frac{1}{6\epsilon_0 \hbar^3} S(\omega_1 + \omega_2) \chi_{12} \chi_{34}, \quad (2)$$

with

$$S(\omega_1 + \omega_2) = \frac{1}{\Omega_{rg} - (\omega_1 + \omega_2)}, \quad (3)$$

$$\chi_{12} = \sum_l \left(\frac{\mu_{rl} \mu_{lg}}{\omega_{lg} - \omega_1} + \frac{\mu_{rl} \mu_{lg}}{\omega_{lg} - \omega_2} \right), \quad (4)$$

$$\chi_{34} = \sum_m \left(\frac{\mu_{rm} \mu_{mg}}{\omega_{mg} - \omega_4} + \frac{\mu_{rm} \mu_{mg}}{\omega_{mg} + \omega_3} \right). \quad (5)$$

Here, $\Omega_{rg} = \omega_{rg} - i\Gamma_r/2$ is the complex transition frequency containing the transition frequency ω_{rg} and the total population decay rate of the r state Γ_r , and μ_{ij} are

the z components of the transition matrix elements coupling states i and j . The summation is performed over all the intermediate states $l(m)$ (namely, states $n^{1,3}P_1$), whose transition frequencies to the ground state g are denoted as $\omega_{lg}(\omega_{mg})$.

$S(\omega_1 + \omega_2)$ describes the shape of the two-photon resonance. In Eq. 3, we do not consider pressure broadening and Doppler broadening for simplicity. The pressure broadening $\Delta\omega_p$ can be included in the expression of the imaginary part of Ω_{rg} by $\Gamma'_r = \Gamma_r + 2\Delta\omega_p$, while the Doppler broadening, which contributes through the Doppler shift of ω_1 and ω_2 , can be introduced by a convolution of $S(\omega_1 + \omega_2)$ with the Maxwell-Boltzmann velocity distribution function (see Supplemental Material [48] for a full mathematical treatment), and dominates the linewidth of $S(\omega_1 + \omega_2)$. Both broadening effects reduce $S(\omega_1 + \omega_2)$, and, consequently, the FWM conversion efficiency. For cadmium vapor with natural abundance, since the isotope shifts are typically larger than or comparable to the Doppler broadening linewidth, $S(\omega_1 + \omega_2)$ should be calculated for each isotope and weighted according to their relative abundances in the summation. To our knowledge, isotope shifts of the $5^1S_0 - 6^1S_0$ transition in cadmium have not been measured. In our computations, we assume the use of pure ^{114}Cd isotope as the nonlinear medium, which is commercially available at a reasonable price. This should result in higher output VUV power than in the natural abundance case [47].

For experimental simplicity, we assume $\omega_1 = \omega_2$, where only two incident laser beams at 375 nm and 710 nm are required to produce the VUV light (see Fig. 1). For the more general case where $\omega_1 \neq \omega_2$, see Supplemental Material [48].

Theoretically, the summation in Eqs. 4 and 5 is carried out over an infinite number of intermediate states. In our calculation, however, the summation is done over 20 intermediate P -states, namely n^1P_1 and n^3P_1 states with $n = 5 - 14$, since the transition matrix elements for high-lying states decrease substantially and the transition frequencies of the corresponding states are detuned from the generated VUV light. Considering the dipole approximation and assuming the linear laser polarization, the selection rules for the coupled states are $\Delta J = \pm 1$ and $\Delta M_J = 0$. All corresponding matrix elements (see Supplemental Material [48]) are calculated using the relativistic Fock-space coupled cluster (FS-CC) method implemented in DIRAC [51, 52] and Exp-T [53, 54] program packages. A more detailed investigation of relativistic and electron correlation effects for high-lying states will be published elsewhere.

The relative contributions to χ_{12} and χ_{34} from various intermediate P -states are shown in Fig. 2. The dominant contributions to χ_{12} and χ_{34} originate from the 5^1P_1 and 6^1P_1 states. For χ_{34} , the 7^1P_1 and 8^1P_1 states each contribute approximately 10%. Contributions from all triplet states and states above the 8^1P_1 to both χ_{12} and χ_{34} are minor.

We choose an incident laser power of 3 W at 375 nm

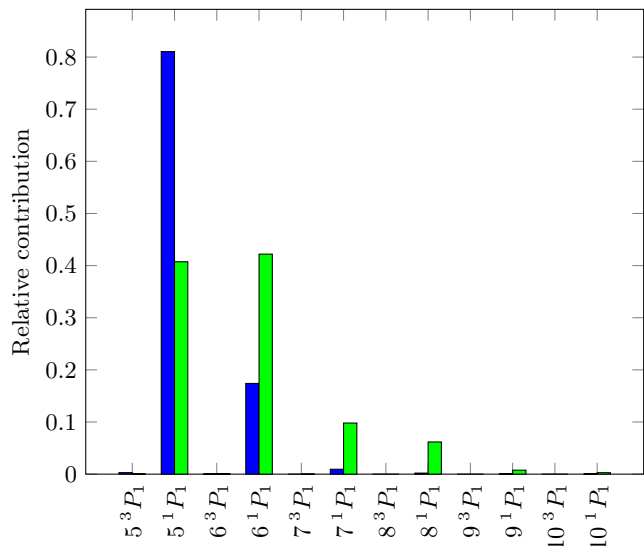


Figure 2. The normalized relative contributions to χ_{12} (blue bars) and χ_{34} (green bars) from a set of intermediate P -states up to the 10^1P_1 .

and 6 W at 710 nm, which are readily available in the laboratory. The confocal parameter is set to $b = 1.5$ mm, and the vapor temperature is set to $T = 580^\circ\text{C}$ to optimize the output VUV power. The saturation vapor pressure as a function of temperature can be found in the Supplemental Material [48]. Under these conditions, we calculate the nonlinear susceptibility $\chi_a^{(3)}$, the phase matching function $G(bN\Delta k_a)$, and the generated VUV power P_4 in the vicinity of Th-229 isomer transition, as shown in Fig. 3.

The nonlinear susceptibility $\chi_a^{(3)}$ exhibits divergence near resonant states since the absorption is not accounted for in Eq. 2. The phase-matching function $G(bN\Delta k_a)$ goes to zero near resonant states because the refractive index of the generated beam is so large that the resulting wave vector mismatch Δk_a cannot be compensated for using the current parameters. The calculated output power P_4 at 148.4 nm is approximately $30 \mu\text{W}$. Zero VUV power points arise when terms with different signs cancel in the χ_{34} expression shown in Eq. 5.

The VUV power can be further enhanced by introducing some noble gas to provide additional compensation for wave vector mismatch, or by tuning one of the incident beams close to the $5^{1,3}P_1$ resonance states, while maintaining two-photon resonance with the second incident beam. For a detailed discussion, see Supplemental Material [48].

We also perform calculations for the FWM scheme exploiting 5^1D_2 as the two-photon resonance state, which is described in detail in the Supplemental Material [48]. Similar to the case with 6^1S_0 as the resonance state, the coupling to 5^1P_1 and 6^1P_1 states dominates the nonlinear susceptibility, and the output VUV power is at comparable level.

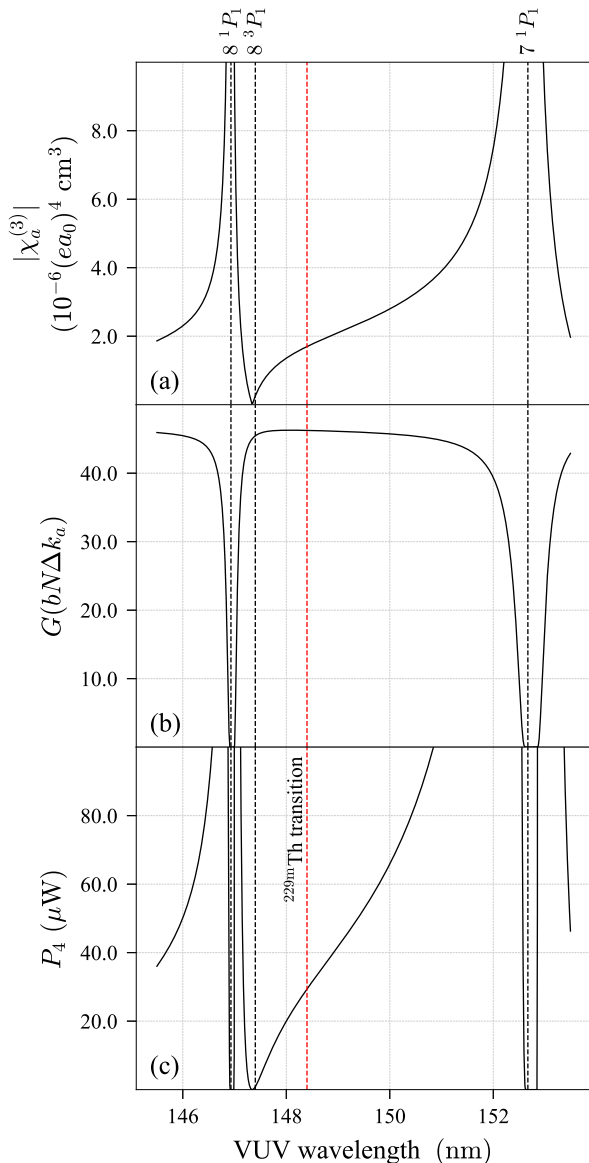


Figure 3. Calculated nonlinear susceptibility $|\chi_a^{(3)}|$, phase matching function $G(bN\Delta k_a)$, and VUV yield P_4 in the vicinity of Th-229 isomer transition according to Eq. 1 using parameters stated in the text. Note that the effects of absorption, saturation are ignored in the plot.

The output VUV power in Fig. 3(c) does not account for absorption and saturation effects. Saturation might be an issue in the tightly focused case, where the laser intensity near the beam waist can be enormous. We find that the only significant saturation effect under the current experimental parameters is due to the depletion of the ground state induced by the two-photon resonance Raman-type absorption [48]. This issue can be mitigated either by slightly detuning the lasers from the exact two-photon resonance condition, or by loosening the focus

while adding some noble gas into the medium for phase mismatch compensation. Other effects, such as the linear absorption of the beams, same order and higher order nonlinear processes, and amplified spontaneous emission are found to be insignificant [48].

As a conservative estimate, we assume a VUV power of $10 \mu\text{W}$ focused to a spot diameter of $8 \mu\text{m}$ to study the interaction of the Th-229 nucleus with the VUV light. This interaction has been treated in detail in [9]. We consider the Th-229 isomer transition as the simplest two-level system interacting with a VUV laser with intensity I_l and linewidth Γ_l . In order to observe nuclear Rabi oscillations, the linewidth of the VUV laser Γ_l needs to satisfy

$$\Gamma_l < 2\Omega_{eg} = 2\sqrt{\frac{2\pi c^2 I_l \Gamma_\gamma}{\hbar \omega_0^3}} \approx 1 \text{ kHz}, \quad (6)$$

where Ω_{eg} is the Rabi frequency, Γ_γ the radiative decay rate of the nuclear excited state, and ω_0 the angular frequency of the isomer transition. The nuclear excitation probability as a function of VUV irradiation time for laser linewidths below and above 1 kHz can be found in the Supplemental Material [48].

We argue that the linewidth condition Eq. 6 can be satisfied in the FWM process. Previously, it has been extensively studied and shown [56–61] that HHG processes in gases are governed by the coherent temporal dynamics of the electron. Advances in VUV frequency comb technology [32, 62, 63] have demonstrated the capability for generating VUV radiation with coherence time greater than 1 s, allowing for sub-hertz spectral resolution for HHG processes. Particularly interesting for the current work is the third harmonic generation [32], which also relies on the third-order nonlinearity, and is a special case of FWM process when $\omega_1 = \omega_2 = \omega_3$. Similar to other noiseless classical frequency multiplications, the phase noise of the incident beams will be scaled up in the FWM process [38], but this incident phase noise can be substantially suppressed by locking the lasers to ultra-stable high-finesse cavities. Therefore, we expect the FWM process to be highly coherent, resulting in VUV light with a linewidth below 1 kHz.

In conclusion, we propose using four-wave mixing in cadmium vapor to generate continuous-wave laser light for precision spectroscopy of the Th-229 isomer transition. Near the Th-229 isomer transition frequency, the nonlinear susceptibility of the employed FWM scheme is large, and the phase-matching condition can be satisfied. With an incident laser power of 3 W at 375 nm and 6 W at 710 nm, more than $30 \mu\text{W}$ of VUV light at 148.4 nm can be produced. The resulting VUV power can be further enhanced by coupling the incident laser beams into a high-finesse cavity to increase the effective incident laser power. The generated VUV light with a sub-kHz linewidth will enable precision spectroscopy of Th-229 isomer transition, the driving of nuclear Rabi oscillations in an ion trap [22, 64, 65], the observation of the

collective effects of nuclear transitions in thorium-doped crystals [66] and the construction of a nuclear optical clock [17, 18]. Additionally, the calculation method can be applied to other nonlinear media to produce VUV light for various applications, such as laser cooling of Al^+ ions and high-resolution atomic and molecular spectroscopy.

While finishing the current work, we became aware of Jun Ye's group's research on Th-229 isomer spectroscopy using a VUV frequency comb, as reported at DAMOP 2024 [67].

ACKNOWLEDGMENTS

We thank Peter Thirolf, Jun Ye, Leonid Skripnikov, Li You and Haoyu Shi for helpful discussions, and Peter Thirolf for carefully reading the manuscript. This work is supported by the National Natural Science Foundation of China (Grants No. 12341401 and No. 12274253) and the National Key Research and Development Program of China (2021YFA1402104).

-
- [1] T. J. Bürvenich, J. Evers, and C. H. Keitel, Nuclear Quantum Optics with X-Ray Laser Pulses, *Phys. Rev. Lett.* **96**, 142501 (2006).
- [2] K. P. Heeg, A. Kaldun, C. Strohm, C. Ott, R. Subramanian, D. Lentrodt, J. Haber, H.-C. Wille, S. Goerttler, R. Ruffer, *et al.*, Coherent X-ray-optical control of nuclear excitons, *Nature* **590**, 401 (2021).
- [3] Y. Shvyd'ko, R. Röhlberger, O. Kocharovskaya, J. Evers, G. A. Geloni, P. Liu, D. Shu, A. Miceli, B. Stone, W. Hippler, *et al.*, Resonant X-ray excitation of the nuclear clock isomer ^{45}Sc , *Nature* **622**, 471 (2023).
- [4] A. Hayes and J. Friar, Sensitivity of nuclear transition frequencies to temporal variation of the fine structure constant or the strong interaction, *Phys. Lett. B* **650**, 229 (2007).
- [5] V. Flambaum, N. Auerbach, and V. Dmitriev, Coulomb energy contribution to the excitation energy in ^{229}Th and enhanced effect of α variation, *Europhys. Lett.* **85**, 50005 (2009).
- [6] L. Kroger and C. Reich, Features of the low-energy level scheme of ^{229}Th as observed in the α -decay of ^{233}U , *Nucl. Phys. A* **259**, 29 (1976).
- [7] C. Reich and R. Helmer, Energy separation of the doublet of intrinsic states at the ground state of ^{229}Th , *Phys. Rev. Lett.* **64**, 271 (1990).
- [8] R. Helmer and C. Reich, An excited state of ^{229}Th at 3.5 eV, *Phys. Rev. C* **49**, 1845 (1994).
- [9] B. Beck, J. Becker, P. Beiersdorfer, G. Brown, K. J. Moody, J. B. Wilhelmy, F. Porter, C. Kilbourne, and R. Kelley, Energy splitting of the ground-state doublet in the nucleus ^{229}Th , *Phys. Rev. Lett.* **98**, 142501 (2007).
- [10] B. Seiferle, L. von der Wense, P. V. Bilous, I. Amersdorfer, C. Lemell, F. Libisch, S. Stellmer, T. Schumm, C. E. Düllmann, A. Pálffy, *et al.*, Energy of the ^{229}Th nuclear clock transition, *Nature* **573**, 243 (2019).
- [11] T. Masuda, A. Yoshimi, A. Fujieda, H. Fujimoto, H. Haba, H. Hara, T. Hiraki, H. Kaino, Y. Kasamatsu, S. Kitao, *et al.*, X-ray pumping of the ^{229}Th nuclear clock isomer, *Nature* **573**, 238 (2019).
- [12] A. Yamaguchi, H. Muramatsu, T. Hayashi, N. Yuasa, K. Nakamura, M. Takimoto, H. Haba, K. Konashi, M. Watanabe, H. Kikunaga, *et al.*, Energy of the ^{229}Th nuclear clock isomer determined by absolute γ -ray energy difference, *Phys. Rev. Lett.* **123**, 222501 (2019).
- [13] T. Sikorsky, J. Geist, D. Hengstler, S. Kempf, L. Gastaldo, C. Enss, C. Mokry, J. Runke, C. E. Düllmann, P. Wobrauschek, *et al.*, Measurement of the ^{229}Th isomer energy with a magnetic microcalorimeter, *Phys. Rev. Lett.* **125**, 142503 (2020).
- [14] S. Kraemer, J. Moens, M. Athanasakis-Kaklamanakis, S. Bara, K. Beeks, P. Chhetri, K. Chrysalidis, A. Claessens, T. E. Cocolios, J. G. Correia, *et al.*, Observation of the radiative decay of the ^{229}Th nuclear clock isomer, *Nature* **617**, 706 (2023).
- [15] J. Tiedau, M. Okhapkin, K. Zhang, J. Thielking, G. Zitzer, E. Peik, F. Schaden, T. Pronebner, I. Morawetz, L. T. De Col, *et al.*, Laser excitation of the Th-229 nucleus, *Phys. Rev. Lett.* **132**, 182501 (2024).
- [16] R. Elwell, C. Schneider, J. Jeet, J. Terhune, H. Morgan, A. Alexandrova, H. Tan, A. Derevianko, and E. R. Hudson, Laser excitation of the ^{229}Th nuclear isomeric transition in a solid-state host, arXiv preprint arXiv:2404.12311 (2024).
- [17] E. Peik and C. Tamm, Nuclear laser spectroscopy of the 3.5 eV transition in Th-229, *Europhys. Lett.* **61**, 181 (2003).
- [18] C. J. Campbell, A. G. Radnaev, A. Kuzmich, V. A. Dzuba, V. V. Flambaum, and A. Derevianko, Single-Ion Nuclear Clock for Metrology at the 19th Decimal Place, *Phys. Rev. Lett.* **108**, 120802 (2012).
- [19] V. V. Flambaum, Enhanced Effect of Temporal Variation of the Fine Structure Constant and the Strong Interaction in ^{229}Th , *Phys. Rev. Lett.* **97**, 092502 (2006).
- [20] J. C. Berengut, V. A. Dzuba, V. V. Flambaum, and S. G. Porsev, Proposed experimental method to determine α sensitivity of splitting between ground and 7.6 eV isomeric states in ^{229}Th , *Phys. Rev. Lett.* **102**, 210801 (2009).
- [21] J. Thielking, M. V. Okhapkin, P. Glowacki, D. M. Meier, L. v. d. Wense, B. Seiferle, C. E. Düllmann, P. G. Thirolf, and E. Peik, Laser spectroscopic characterization of the nuclear-clock isomer $^{229\text{m}}\text{Th}$, *Nature* **556**, 321 (2018).
- [22] A. Yamaguchi, Y. Shigekawa, H. Haba, H. Kikunaga, K. Shirasaki, M. Wada, and H. Katori, Laser spectroscopy of triply charged ^{229}Th isomer for a nuclear clock, *Nature* **629**, 62 (2024).
- [23] A. Arvanitaki, J. Huang, and K. Van Tilburg, Searching for dilaton dark matter with atomic clocks, *Phys. Rev. D* **91**, 015015 (2015).
- [24] Y.-D. Tsai, J. Eby, and M. S. Safronova, Direct detection of ultralight dark matter bound to the Sun with space quantum sensors, *Nat. Astron.* **7**, 113 (2023).
- [25] W. G. Rellergert, D. DeMille, R. R. Greco, M. P. Hehlen, J. Torgerson, and E. R. Hudson, Constraining the Evolution of the Fundamental Constants with a Solid-State Optical Frequency Reference Based on the ^{229}Th Nucleus, *Phys. Rev. Lett.* **104**, 200802 (2010).

- [26] G. Kazakov, A. Litvinov, V. Romanenko, L. Yatsenko, A. Romanenko, M. Schreitl, G. Winkler, and T. Schumm, Performance of a ^{229}Th solid-state nuclear clock, *New J. Phys.* **14**, 083019 (2012).
- [27] P. Thirolf, B. Seiferle, and L. Von der Wense, The ^{229}Th isomer: doorway to the road from the atomic clock to the nuclear clock, *J. Phys. B At. Mol. Opt. Phys.* **52**, 203001 (2019).
- [28] E. Peik, T. Schumm, M. Safronova, A. Palffy, J. Weitenberg, and P. G. Thirolf, Nuclear clocks for testing fundamental physics, *Quantum Sci. Technol.* **6**, 034002 (2021).
- [29] K. Beeks, T. Sikorsky, T. Schumm, J. Thielking, M. V. Okhapkin, and E. Peik, The thorium-229 low-energy isomer and the nuclear clock, *Nat. Rev. Phys.* **3**, 238 (2021).
- [30] L. v. d. Wense, B. Seiferle, M. Laatiaoui, J. B. Neumayr, H. Maier, H. Wirth, C. Mokry, J. Runke, K. Eberhardt, C. E. Düllmann, N. G. Trautmann, and P. G. Thirolf, Direct detection of the ^{229}Th nuclear clock transition, *Nature* **533**, 47 (2016).
- [31] T. Hiraki, K. Okai, M. Bartokos, K. Beeks, H. Fujimoto, Y. Fukunaga, H. Haba, Y. Kasamatsu, S. Kitao, A. Leitner, *et al.*, Controlling ^{229}Th isomeric state population in a VUV transparent crystal, arXiv preprint arXiv:2405.09577 (2024).
- [32] R. Jones, K. Moll, M. Thorpe, and J. Ye, Phase-Coherent Frequency Combs in the Vacuum Ultraviolet via High-Harmonic Generation inside a Femtosecond Enhancement Cavity, *Phys. Rev. Lett.* **94** (2005).
- [33] C. Gohle, T. Udem, M. Herrmann, J. Rauschenberger, R. Holzwarth, H. A. Schuessler, F. Krausz, and T. W. Hänsch, A frequency comb in the extreme ultraviolet, *Nature* **436**, 234 (2005).
- [34] I. Pupeza, C. Zhang, M. Högner, and J. Ye, Extreme-ultraviolet frequency combs for precision metrology and attosecond science, *Nat. Photon.* **15**, 175 (2021).
- [35] L. von der Wense, B. Seiferle, S. Stellmer, J. Weitenberg, G. Kazakov, A. Pálffy, and P. G. Thirolf, A Laser Excitation Scheme for $^{229\text{m}}\text{Th}$, *Phys. Rev. Lett.* **119**, 132503 (2017).
- [36] J. Seres, E. Seres, C. Serrat, E. Young, J. Speck, and T. Schumm, All-solid-state VUV frequency comb at 160 nm using high-harmonic generation in nonlinear femtosecond enhancement cavity, *Opt. Express* **27**, 6618 (2019).
- [37] C. Zhang, P. Li, J. Jiang, L. von der Wense, J. F. Doyle, M. E. Fermann, and J. Ye, Tunable VUV frequency comb for $^{229\text{m}}\text{Th}$ nuclear spectroscopy, *Opt. Lett.* **47**, 5591 (2022).
- [38] J. Thielking, K. Zhang, J. Tiedau, J. Zander, G. Zitzer, M. Okhapkin, and E. Peik, Vacuum-ultraviolet laser source for spectroscopy of trapped thorium ions, *New J. Phys.* **25**, 083026 (2023).
- [39] J. Jeet, *Search for the Low Lying Transition in the ^{229}Th Nucleus* (University of California, Los Angeles, 2018).
- [40] P. Thirolf, Shedding Light on the Thorium-229 Nuclear Clock Isomer, *Physics* **17**, 71 (2024).
- [41] R. Hodgson, P. Sorokin, and J. J. Wynne, Tunable Coherent Vacuum-Ultraviolet Generation in Atomic Vapors, *Phys. Rev. Lett.* **32**, 343 (1974).
- [2] C. R. Vidal, *Four-Wave Frequency Mixing in Gases* (Springer, 2005) Chap. 3.
- [43] K. Eikema, J. Walz, and T. Hänsch, Continuous Wave Coherent Lyman- α Radiation, *Phys. Rev. Lett.* **83**, 3828 (1999).
- [44] K. Eikema, J. Walz, and T. Hänsch, Continuous Coherent Lyman- α Excitation of Atomic Hydrogen, *Phys. Rev. Lett.* **86**, 5679 (2001).
- [45] D. Kolbe, M. Scheid, and J. Walz, Triple Resonant Four-Wave Mixing Boosts the Yield of Continuous Coherent Vacuum Ultraviolet Generation, *Phys. Rev. Lett.* **109**, 063901 (2012).
- [3] B. Gary C, Effects of focusing on third-order nonlinear processes, *IEEE J. Quantum Electron.* **QE-11**, 287 (1975).
- [47] A. Pahl, P. Fendel, B. R. Henrich, J. Walz, T. W. Hänsch, and K. S. E. Eikema, Generation of continuous coherent radiation at Lyman- α and 1s-2p spectroscopy of atomic hydrogen, *Laser Phys.* **15**, 46 (2005).
- [48] See Supplemental Material at [URL will be inserted by publisher], which also includes Refs. [50-56].
- [49] R. W. Boyd, *Nonlinear Optics, Third Edition* (Academic Press, Inc., 2008).
- [4] A. V. Smith and W. J. Alford, Practical guide for 7S resonant frequency mixing in mercury: generation of light in the 230-185- and 140-120-nm ranges, *J. Opt. Soc. Am. B* **4**, 1765 (1987).
- [51] DIRAC, a relativistic ab initio electronic structure program, Release DIRAC19 (2019), written by A. S. P. Gomes, T. Saue, L. Visscher, H. J. Aa. Jensen, and R. Bast, with contributions from I. A. Aucar, V. Bakken, K. G. Dyall, S. Dubillard, U. Ekstroem, E. Eliav, T. Enevoldsen, E. Fasshauer, T. Fleig, O. Fossgaard, L. Halbert, E. D. Hedegaard, T. Helgaker, J. Henriksson, M. Ilias, Ch. R. Jacob, S. Knecht, S. Komorovsky, O. Kullie, J. K. Laerdahl, C. V. Larsen, Y. S. Lee, H. S. Nataraj, M. K. Nayak, P. Norman, M. Olejniczak, J. Olsen, J. M. H. Olsen, Y. C. Park, J. K. Pedersen, M. Pernpointner, R. Di Remigio, K. Ruud, P. Salek, B. Schimelpennig, B. Senjean, A. Shee, J. Sikkema, A. J. Thorvaldsen, J. Thyssen, J. van Stralen, M. L. Vidal, S. Villaume, O. Visser, T. Winther, and S. Yamamoto (see <http://diracprogram.org>).
- [52] T. Saue, R. Bast, A. S. P. Gomes, H. J. A. Jensen, L. Visscher, I. A. Aucar, R. Di Remigio, K. G. Dyall, E. Eliav, E. Fasshauer, T. Fleig, L. Halbert, E. D. Hedegaard, B. Helmich-Paris, M. Ilias, C. R. Jacob, S. Knecht, J. K. Laerdahl, M. L. Vidal, M. K. Nayak, M. Olejniczak, J. M. H. Olsen, M. Pernpointner, B. Senjean, A. Shee, A. Sunaga, and J. N. P. van Stralen, The dirac code for relativistic molecular calculations, *J. Comp. Phys.* **152**, 204104 (2020).
- [53] A. V. Oleynichenko, A. Zaitsevskii, and E. Eliav, Towards high performance relativistic electronic structure modelling: the EXP-T program package, in *Supercomputing*, Vol. 1331, edited by V. Voevodin and S. Sobolev (Springer International Publishing, Cham, 2020) pp. 375–386.
- [54] A. Oleynichenko, A. Zaitsevskii, and E. Eliav, (2021), EXP-T, an extensible code for Fock space relativistic coupled cluster calculations (see <http://www.qchem.pnpi.spb.ru/expt>).
- [9] L. von der Wense, P. V. Bilous, B. Seiferle, S. Stellmer, J. Weitenberg, P. G. Thirolf, A. Pálffy, and G. Kazakov, The theory of direct laser excitation of nuclear transitions, *The European Physical Journal A* **56**, 1 (2020).
- [56] A. L’Huillier, M. Lewenstein, P. Salières, P. Balcou, M. Y. Ivanov, J. Larsson, and C. G. Wahlström, High-order Harmonic-generation cutoff, *Phys. Rev. A* **48**, R3433 (1993).
- [57] M. Lewenstein, P. Salières, and A. L’Huillier, Phase of

- the atomic polarization in high-order harmonic generation, *Phys. Rev. A* **52**, 4747 (1995).
- [58] C. Corsi, A. Pirri, E. Sali, A. Tortora, and M. Bellini, Direct Interferometric Measurement of the Atomic Dipole Phase in High-Order Harmonic Generation, *Phys. Rev. Lett.* **97**, 023901 (2006).
- [59] W.-H. Xiong, J.-W. Geng, J.-Y. Tang, L.-Y. Peng, and Q. Gong, Mechanisms of below-threshold harmonic generation in atoms, *Phys. Rev. Lett.* **112**, 233001 (2014).
- [60] A. V. F. Zuffi, N. D. Vieira Junior, and R. E. Samad, Below-threshold-harmonics-generation limitation due to laser-induced ionization in noble gases, *Phys. Rev. A* **105**, 023112 (2022).
- [61] P.-C. Li, Y.-L. Sheu, C. Laughlin, and S.-I. Chu, Dynamical origin of near- and below-threshold harmonic generation of Cs in an intense mid-infrared laser field, *Nat. Commun.* **6**, 7178 (2015).
- [62] D. C. Yost, T. R. Schibli, J. Ye, J. L. Tate, J. Hostetter, M. B. Gaarde, and K. J. Schafer, Vacuum-ultraviolet frequency combs from below-threshold harmonics, *Nat. Phys.* **5**, 815 (2009).
- [63] C. Benko, T. K. Allison, A. Cingoz, L. Hua, F. Labaye, D. C. Yost, and J. Ye, Extreme ultraviolet radiation with coherence time greater than 1 s, *Nat. Photon.* **8**, 530 (2014).
- [64] C. J. Campbell, A. G. Radnaev, and A. Kuzmich, Wigner crystals of ^{229}Th for optical excitation of the nuclear isomer, *Phys. Rev. Lett.* **106**, 223001 (2011).
- [65] G. Zitzer, J. Tiedau, M. V. Okhapkin, K. Zhang, C. Mokry, J. Runke, C. E. Düllmann, and E. Peik, Sympathetic cooling of trapped Th^{3+} alpha-recoil ions for laser spectroscopy, *Phys. Rev. A* **109**, 033116 (2024).
- [66] B. S. Nickerson, W.-T. Liao, and A. Pálffy, Collective effects in ^{229}Th -doped crystals, *Phys. Rev. A* **98**, 062520 (2018).
- [67] C. Zhang *et al.*, Connecting a narrow Th-229 nuclear clock transition with Sr optical clock via a VUV frequency comb (2024), 55th Annual Meeting of the APS Division of Atomic, Molecular and Optical Physics.

SUPPLEMENTAL MATERIAL

A. 5^1D_2 as the two-photon resonance state

We have also performed calculations for the case with 5^1D_2 as the two-photon resonance state. For $\omega_1 = \omega_2$, the incident lasers are 338 nm and 1223 nm, as shown in Fig. 4.

The relative contributions to χ_{12} and χ_{34} stemming from different intermediate P -states are presented in Fig. 5. Similar to the case with 6^1S_0 as the two-photon resonance state, the coupling to the 5^1P_1 and 6^1P_1 states dominates the nonlinear susceptibility, and contributions from all triplet states and states above 8^1P_1 are negligible.

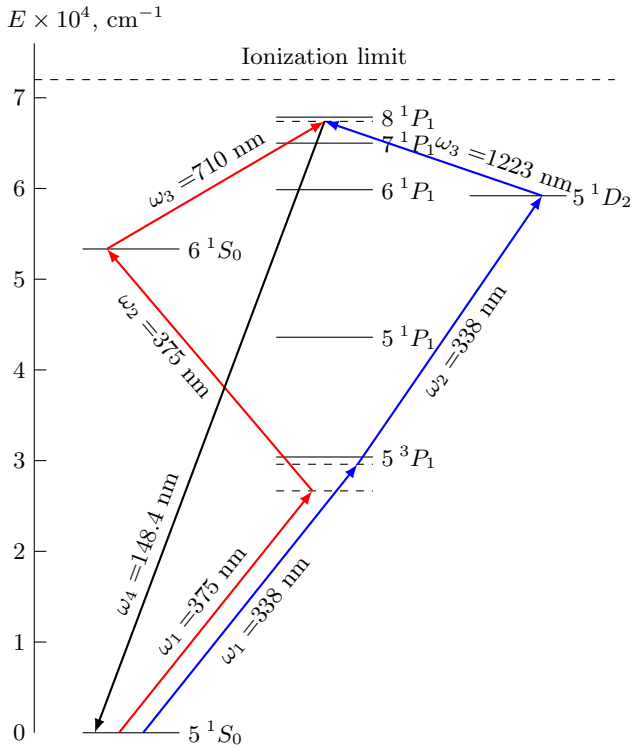


Figure 4. Simplified energy level scheme of neutral Cd. The red and blue arrows represent the incident lasers ω_1 , ω_2 , ω_3 with 6^1S_0 and 5^1D_2 as two-photon resonance states, respectively. The black arrow indicates the generated VUV laser at 148.4 nm.

The calculated phase matching function $G(bN\Delta k_a)$, the nonlinear susceptibility $\chi_a^{(3)}$, and the generated VUV power P_4 in the vicinity of Th-229 isomer transition are shown in Fig. 6. The optimal phase matching temperature is $T = 570$ °C for $b = 1.5$ mm. With the same laser powers (3 W at 338 nm and 6 W at 1223 nm), around half of the VUV power can be generated compared to the case exploiting 6^1S_0 as the two-photon resonance state. Nevertheless, the power of the commercially available 1223 nm laser can be as high as 30 W, making the

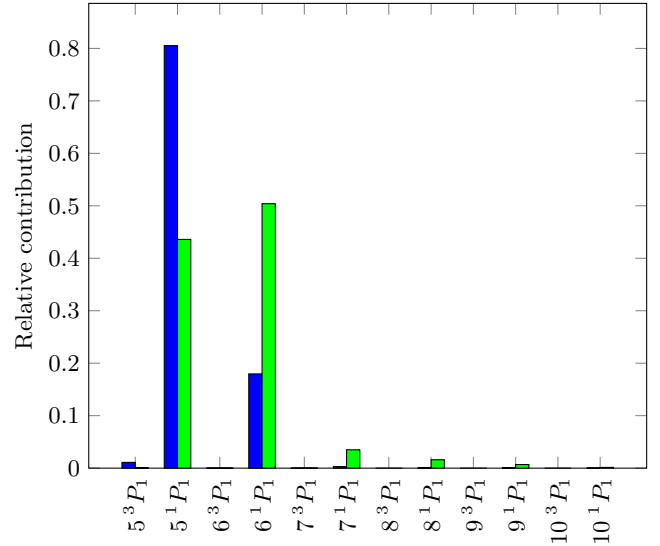


Figure 5. The normalized relative contributions to χ_{12} (blue bars) and χ_{34} (green bars) for the scheme exploiting the 5^1D_2 as the two-photon resonance state from a set of intermediate P -states up to 10^1P_1 .

5^1D_2 scheme also appealing.

B. Phase matching

It can be shown that the wave vector mismatch $\Delta k_a = (k_4 - k_1 - k_2 - k_3)/N$ is independent of the number density of the nonlinear medium N . The wave vector k_i is related to the refractive index $n(\omega_i)$ by

$$k_i = n(\omega_i)\omega_i/c, \quad (7)$$

where [1]

$$n(\omega_i) \simeq 1 + \frac{1}{2}\text{Re}[\chi^{(1)}] = 1 + \frac{Ne^2}{2\epsilon_0 m_e} \sum_m \frac{f_{mg}}{\omega_{mg}^2 - \omega_i^2}. \quad (8)$$

Here f_{mg} and ω_{mg} are the oscillator strength and transition frequency, respectively. The oscillator strength f_{mg} is given by [1]

$$f_{mg} = \frac{2m\omega_{mg}|\boldsymbol{\mu}_{mg}|^2}{3\hbar e^2}, \quad (9)$$

with the dipole moment matrix element $\boldsymbol{\mu}_{mg}$ related to its z component μ_{mg} by Wigner-Eckart Theorem [2].

By making use of expression $\omega_1 + \omega_2 + \omega_3 = \omega_4$, we get

$$\Delta k_a = \frac{e^2}{2\epsilon_0 m_e c} \sum_m \left(\frac{f_{mg}\omega_4}{\omega_{mg}^2 - \omega_4^2} - \sum_{j=1,2,3} \frac{f_{mg}\omega_j}{\omega_{mg}^2 - \omega_j^2} \right). \quad (10)$$

Therefore, Δk_a does not depend on the number density of the nonlinear medium, but the frequencies of incident and generated lasers.

Table I. Values of reduced E1 matrix elements for neutral Cd used in the calculation of the nonlinear susceptibility.

Transition	d, a.u.	Transition	d, a.u.	Transition	d, a.u.
$5s^1S_0 \rightarrow 5^3P_1$	0.148	$5^3P_1 \rightarrow 6^1S_0$	0.082	$5^3P_1 \rightarrow 5^1D_2$	0.138
$5^1S_0 \rightarrow 5^1P_1$	3.461	$5^1P_1 \rightarrow 6^1S_0$	4.199	$5^1P_1 \rightarrow 5^1D_2$	5.673
$5^1S_0 \rightarrow 6^3P_1$	0.013	$6^1S_0 \rightarrow 6^3P_1$	0.696	$6^3P_1 \rightarrow 5^1D_2$	0.111
$5^1S_0 \rightarrow 6^1P_1$	0.769	$6^1S_0 \rightarrow 6^1P_1$	7.919	$5^1D_2 \rightarrow 6^1P_1$	12.241
$5^1S_0 \rightarrow 7^3P_1$	0.001	$6^1S_0 \rightarrow 7^3P_1$	0.021	$5^1D_2 \rightarrow 7^3P_1$	0.069
$5^1S_0 \rightarrow 7^1P_1$	0.327	$6^1S_0 \rightarrow 7^1P_1$	1.175	$5^1D_2 \rightarrow 7^1P_1$	0.552
$5^1S_0 \rightarrow 8^3P_1$	0.0004	$6^1S_0 \rightarrow 8^3P_1$	0.007	$5^1D_2 \rightarrow 8^3P_1$	0.034
$5^1S_0 \rightarrow 8^1P_1$	0.196	$6^1S_0 \rightarrow 8^1P_1$	0.441	$5^1D_2 \rightarrow 8^1P_1$	0.149
$5^1S_0 \rightarrow 9^3P_1$	0.0003	$6^1S_0 \rightarrow 9^3P_1$	0.010	$5^1D_2 \rightarrow 9^3P_1$	0.020
$5^1S_0 \rightarrow 9^1P_1$	0.136	$6^1S_0 \rightarrow 9^1P_1$	0.237	$5^1D_2 \rightarrow 9^1P_1$	0.27
$5^1S_0 \rightarrow 10^3P_1$	0.0003	$6^1S_0 \rightarrow 10^3P_1$	0.009	$5^1D_2 \rightarrow 10^3P_1$	0.003
$5^1S_0 \rightarrow 10^1P_1$	0.106	$6^1S_0 \rightarrow 10^1P_1$	0.157	$5^1D_2 \rightarrow 10^1P_1$	0.099
$5^1S_0 \rightarrow 11^3P_1$	0.0002	$6^1S_0 \rightarrow 11^3P_1$	0.006	$5^1D_2 \rightarrow 11^3P_1$	0.007
$5^1S_0 \rightarrow 11^1P_1$	0.081	$6^1S_0 \rightarrow 11^1P_1$	0.112	$5^1D_2 \rightarrow 11^1P_1$	0.038
$5^1S_0 \rightarrow 12^3P_1$	0.0003	$6^1S_0 \rightarrow 12^3P_1$	0.003	$5^1D_2 \rightarrow 12^3P_1$	0.005
$5^1S_0 \rightarrow 12^1P_1$	0.050	$6^1S_0 \rightarrow 12^1P_1$	0.070	$5^1D_2 \rightarrow 12^1P_1$	0.012
$5^1S_0 \rightarrow 13^3P_1$	0.0005	$6^1S_0 \rightarrow 13^3P_1$	0.001	$5^1D_2 \rightarrow 13^3P_1$	0.003
$5^1S_0 \rightarrow 13^1P_1$	0.028	$6^1S_0 \rightarrow 13^1P_1$	0.041	$5^1D_2 \rightarrow 13^1P_1$	0.003
$5^1S_0 \rightarrow 14^3P_1$	0.0005	$6^1S_0 \rightarrow 14^3P_1$	0.0006	$5^1D_2 \rightarrow 14^3P_1$	0.002
$5^1S_0 \rightarrow 14^1P_1$	0.017	$6^1S_0 \rightarrow 14^1P_1$	0.027	$5^1D_2 \rightarrow 14^1P_1$	0.001

The phase-matching function in the tight focus limit can be written explicitly as [3]

$$G(bN\Delta k_a) = G(b\Delta k) = \begin{cases} 0 & \text{for } b\Delta k > 0, \\ \pi^2(b\Delta k)^4 e^{b\Delta k} & \text{for } b\Delta k < 0, \end{cases} \quad (11)$$

where we define $\Delta k = k_4 - k_1 - k_2 - k_3 = N\Delta k_a$. The function above attains its maximum value at $b\Delta k = -4$.

C. Calculation of $S(\omega_1 + \omega_2)$

The pressure broadening and Doppler broadening are typically much larger than the natural linewidth of the two-photon resonance state, and must be considered for the calculation of $S(\omega_1 + \omega_2)$. The pressure broadening $\Delta\omega_p$ is expressed as

$$\Delta\omega_p = Nd^2 \sqrt{\frac{16\pi k_b T}{m}}, \quad (12)$$

where d and m are the kinetic diameter and the atomic mass of the nonlinear medium atom, respectively, T the medium temperature. For the calculation of $S(\omega_1 + \omega_2)$, pressure broadening can be directly added to the population decay rate Γ_r by

$$\Gamma_r' = \Gamma_r + 2\Delta\omega_p, \quad (13)$$

since the decoherence of the collisional dephasing and the damping of the natural decay both contribute to decoherence of the transition. This results in a decrease of the FWM conversion efficiency.

The Doppler broadening is given by

$$\Delta\omega_D = 2\pi\omega_{rg} \sqrt{\frac{8k_b T \ln 2}{mc^2}}. \quad (14)$$

It can be accounted for by using the Maxwell-Boltzmann distribution to collect contributions from atoms with different velocities [4]

$$S(\omega_1 + \omega_2) = \int_{-\infty}^{+\infty} \frac{1}{\Omega_{rg} - \omega_1' - \omega_2'} f(v_x) dv_x. \quad (15)$$

Here $\omega_i' = \omega_i(1 + \frac{v_x}{c})$ is the angular frequency in the atom frame moving with a longitudinal velocity v_x towards the i^{th} incident beam, and $f(v_x)dv_x$ is the Maxwell-Boltzmann velocity distribution given by

$$f(v_x)dv_x = \sqrt{\frac{m}{2\pi kT}} \exp\left(-\frac{mv_x^2}{2kT}\right) dv_x. \quad (16)$$

Substituting Eq. 13, Eq. 14 and Eq. 16 into Eq. 15 and performing non-dimensionalization, we get [4]

$$S(\omega_1 + \omega_2) = \frac{1}{w} Z(\zeta). \quad (17)$$

Here $Z(\zeta)$ is the plasma-dispersion function given by

$$Z(\zeta) = \frac{1}{\sqrt{\pi}} \int_{-\infty}^{+\infty} dx \frac{e^{-x^2}}{x - \zeta}, \quad (18)$$

$$\zeta = \left(\omega_1 + \omega_2 + i\frac{\Gamma_r'}{2} - \omega_{rg}\right)/w, \quad (19)$$

$$w = \frac{\Delta\omega_D}{2\sqrt{\ln 2}}. \quad (20)$$

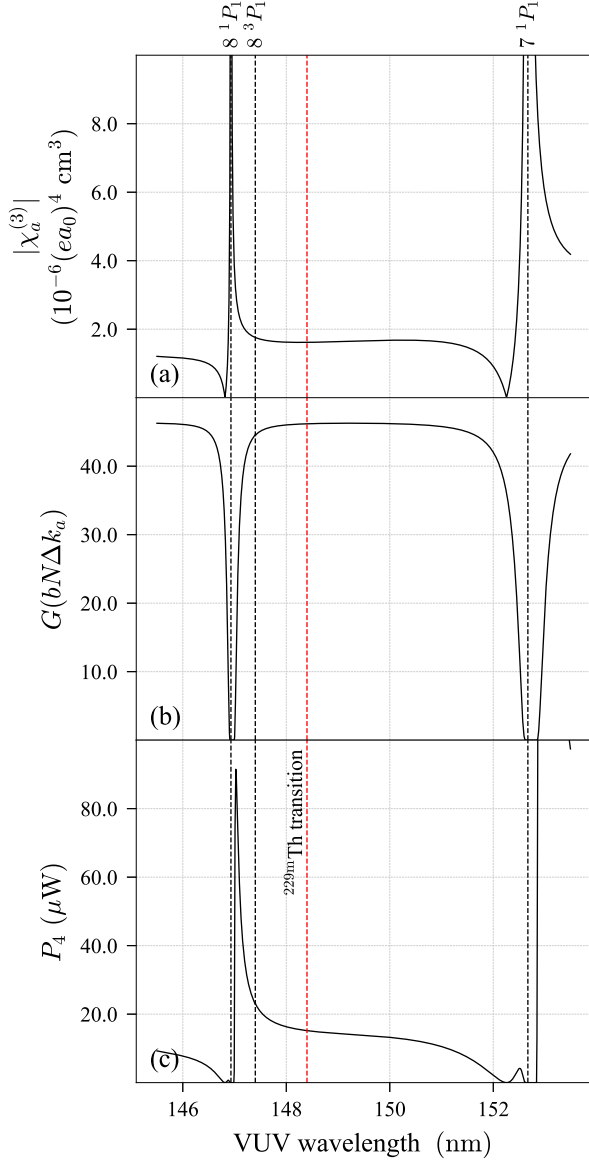


Figure 6. The calculated nonlinear susceptibility $|\chi_a^{(3)}|$, the phase matching function $G(bN\Delta k_a)$, and the VUV yield P_4 in the vicinity of Th-229 isomer transition with the 5^1D_2 as the two-photon resonance state. The confocal parameter is $b = 1.5$ mm, the temperature is $T = 570$ °C, and the power of the incident beams is 3 W for the 338 nm beam and 6 W for the 1223 nm beam.

Moving atoms experience detuning from the two-photon resonance condition, and contribute less to the value of $S(\omega_1 + \omega_2)$. This leads to a Doppler-broadening-induced decrease of FWM conversion efficiency.

Note that $S(\omega_1 + \omega_2)$ has a weak correlation with the number density of the nonlinear medium N , since both the pressure broadening and the Doppler broadening depend on the medium temperature, which in turn dic-

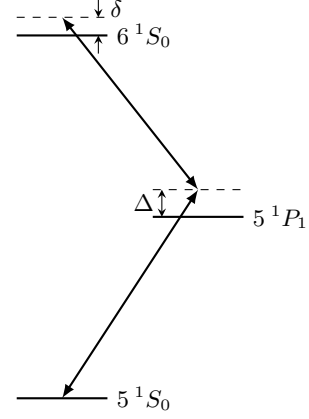


Figure 7. $5^1S_0 - 6^1S_0$ Raman-type transition.

tates the number density of the nonlinear medium N . Therefore, the optimal output power requires a phase-matching condition slightly deviating from the optimal phase-matching condition $b\Delta k = -4$ solely determined by optimizing $G(bN\Delta k_a)$.

D. Saturation and absorption effects

In the calculation of the VUV power according to Eq. 1 in the main text, we assume the small signal limit, which is only valid when saturation and linear absorption effects are negligible. Saturation is defined as the deviation from the relation $P_4 \propto P_1 P_2 P_3$, which holds only when the intensities of the incident and generated beams are low.

At high incident laser intensities, two-photon resonance Raman-type absorption becomes significant, pumping the population from the 5^1S_0 state to the 6^1S_0 state. The depletion of the ground state reduces the third order nonlinear susceptibility $\chi_a^{(3)}$, thereby decreasing the output power. On the other hand, if the population in the 6^1S_0 state becomes sufficiently high to form a population inversion between the 6^1S_0 and the 5^1P_1 states, amplified spontaneous emission (ASE) may occur. ASE broadens the 6^1S_0 state, reducing the $S(\omega_1 + \omega_2)$ factor and the output power. Additionally, the altered population distribution changes the refractive index n , potentially disrupting the phase-matching condition.

Other saturation mechanisms, such as absorption and refractive index changes induced by third-order and higher-order processes, as well as pump depletion arising from competing processes, are estimated to be negligible in our case [5].

1. Population introduced by two-photon absorption

We adiabatically eliminate the intermediate states, and reduce the three level system to a two level system (see

Fig. 7). The two-photon Rabi frequency is

$$\Omega = \frac{\Omega_1 \Omega_2}{2\Delta}, \quad (21)$$

where $\Omega_{1,2}$ are the single-photon Rabi frequencies, and Δ is the detuning from the 5^1P_1 state. We neglect the coupling through other intermediate P -states.

The population of the two-photon resonance state 6^1S_0 is estimated as [6]

$$\rho_{ee} = \frac{\Omega^2/2}{\Omega^2 + \frac{2\Gamma_r}{\Gamma_r}(\delta^2 + \Gamma_r'^2/4)}, \quad (22)$$

where δ is the two-photon detuning, Γ_r is the total population decay rate and Γ_r' includes the pressure broadening effect.

With 3 W laser power at 375 nm, 6 W at 710 nm, and $b = 1.5$ mm, we estimate the 6^1S_0 excited state population to be 12%, indicating a severe saturation effect. This effect can be eliminated by slightly detuning the lasers from the two-photon resonance, for example, by $\delta = 2\pi \times 400$ MHz. With this detuning, the population in the 6^1S_0 excited state reduces to a negligible value of 0.36%, while $S(\omega_1 + \omega_2)$ remains largely unchanged (see Fig. 8).

2. Amplified spontaneous emission (ASE) effects

The population inversion between the 6^1S_0 state and the lower-lying $5^{1,3}P_1$ states can cause amplified spontaneous emission. This is another possible source of saturation, which can be represented by a diagram in Fig. 9.

For relatively small laser intensities, the ASE broadening can be accounted for by replacing the Doppler width in Eq. 17 by [4]:

$$\Delta\omega_D \rightarrow (\Delta\omega_D^2 + \Delta\omega_{\text{ASE}}^2)^{1/2}, \quad (23)$$

where $\Delta\omega_{\text{ASE}}$ is the power-broadened width associated with the ASE.

To estimate the possible broadening caused by the ASE process for the 6^1S_0 state, we follow a derivation in Ref. [7]. For a Lorentzian line, the ASE intensity is given by:

$$I_{\text{ASE}} = \phi I_s \left(\frac{\Omega}{4\pi} \right) \frac{(G-1)^{3/2}}{(G \ln G)^{1/2}}. \quad (24)$$

Here I_s is the saturation intensity, ϕ the fluorescence quantum yield, Ω the emission solid angle, and G the gain of the active medium. We assume the active medium length to be twice the Rayleigh range, and use the parameters in last section to calculate the two-photon Rabi frequency. The power-broadened width associated with the ASE is estimated [8] to be $\Delta\omega_{\text{ASE}} \approx 25$ MHz, which is negligible compared to the Doppler width.

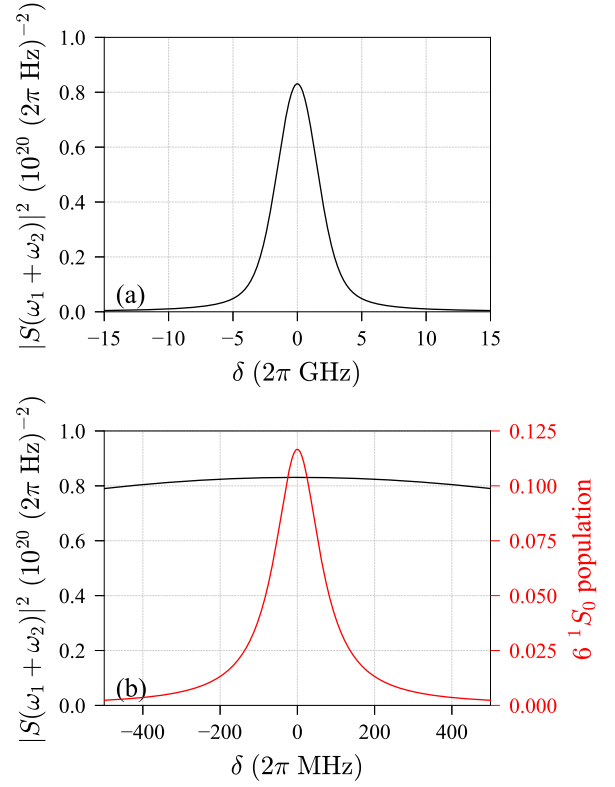


Figure 8. (a) The calculated $|S(\omega_1 + \omega_2)|^2$ with 5^1S_0 as the two-photon resonance state. The linewidth is $2\pi \times 4$ GHz, dominated by the Doppler broadening. (b) The 6^1S_0 state population as a function of two-photon detuning δ , shown by the red line. It is compared to the $(|S(\omega_1 + \omega_2)|^2)$, shown by the black line. A detuning of $\delta = 2\pi \times 400$ MHz suppresses the 6^1S_0 state population without hindering $|S(\omega_1 + \omega_2)|^2$.

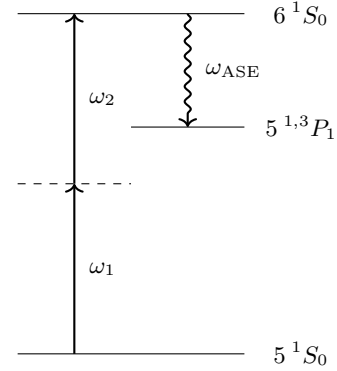


Figure 9. Amplified spontaneous emission process.

3. Linear absorption of the beams

Linear absorption is typically negligible. However, if any of the waves are close to the resonant states, or if the nonlinear medium vapor zone is very long, linear absorption should be considered. The saturated vapour pres-

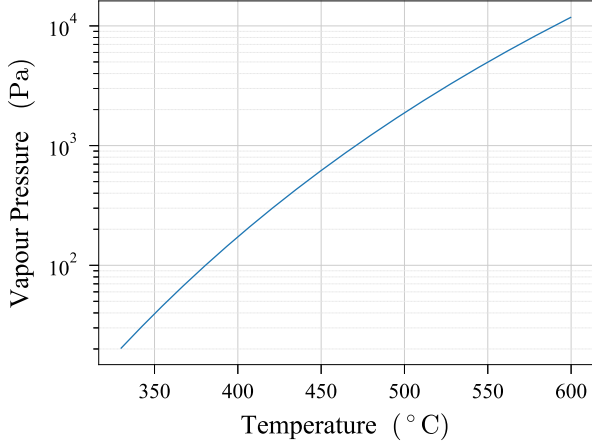


Figure 10. Cadmium vapour pressure. Typically, we get 8500 Pa of cadmium at 580 °C.

sure of cadmium as a function of temperature is shown in Fig. 10. The calculated absorption cross section for different wavelengths is plotted in Fig. 11. The absorption cross section is negligible at 375 nm. At 148.4 nm, it amounts to 0.045 cm^{-1} , and can be neglected for short medium length.

E. Noble gas for phase matching

At around 148.4 nm, cadmium is negatively dispersive, where the refractive index is smaller at smaller wavelengths. If the required confocal parameter b for a high output VUV power is too small to be practical, one could exploit the positive dispersion of noble gases for wave vector mismatch compensation [4]. This extra compensation can also be employed to loose the focus (i.e., enlarge b) such that the saturation effect due to the high light intensity in the focus can be mitigated. Our calculations show that krypton and xenon gases are good choices for this purpose. For the confocal parameter $b = 1.5 \text{ mm}$ adopted in the main text, adding a certain amount of krypton gas could improve the VUV power from $30 \mu\text{W}$ to $50 \mu\text{W}$.

F. When $\omega_1 \neq \omega_2$

By tuning ω_1 close to the $5^{1,3}P_1$ resonance states while keeping the two-photon resonance condition ($\omega_1 + \omega_2$ remains unchanged), the output VUV power can be improved. In this case, the phase matching becomes challenging as the refractive index deviates significantly from unity. The resulting wave vector mismatch can be compensated by lowering the medium's density N or by adding some noble gas. The output VUV power can be

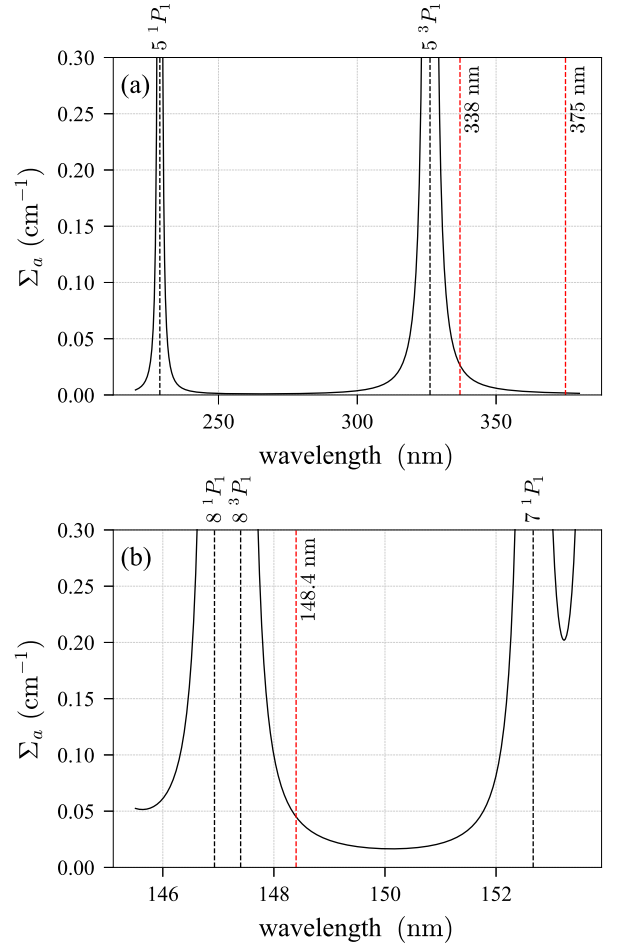


Figure 11. Absorption cross section (in cm^{-1}) in the wavelength vicinity of the (a) input beams, (b) output VUV beam, calculated for $N = 7.2 \times 10^{17} \text{ cm}^{-3}$, or $T = 580 \text{ °C}$.

enhanced by several times and is highly sensitive to input parameters and medium conditions.

G. Theory of the optical nuclear excitation

The interaction of the Th-229 nucleus with the VUV light has been treated in [9]. For simplicity, we consider a nuclear two-level system consisting of a ground state g and an excited state e . The laser-induced Rabi frequency Ω_{eg} can be written as

$$\Omega_{eg} = \sqrt{\frac{2\pi c^2 I_l \Gamma_\gamma}{\hbar \omega_0^3}}, \quad (25)$$

where I_l is the laser intensity, ω_0 the angular frequency of the nuclear transition, and Γ_γ the radiative decay rate of the nuclear excited state.

For an extremely low excited state decay rate, as in the case of the Th-229 isomer transition, the condition for the

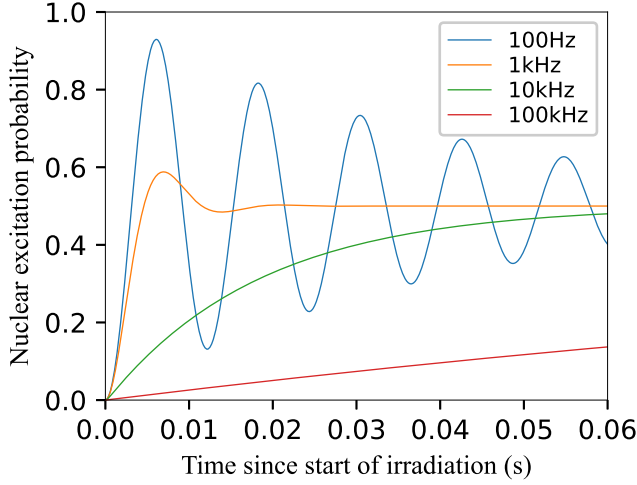


Figure 12. The time-dependent nuclear excitation probability for a single Th-229 nucleus as a function of resonant irradiation time for different laser linewidths.

VUV laser linewidth Γ_l to observe the Rabi oscillation can be written as

$$\Gamma_l < 2\Omega_{eg} = 2\sqrt{\frac{2\pi c^2 I_l \Gamma_\gamma}{\hbar \omega_0^3}}. \quad (26)$$

We assume the VUV laser with a power of 10 μW is focused to a spot diameter of 8 μm . To observe the nuclear Rabi oscillation, the VUV laser linewidth needs to satisfy

$$\Gamma_l < 1 \text{ kHz}. \quad (27)$$

The nuclear excitation probability as a function of irradiation time for different laser linewidths is plotted in Fig. 12. As expected, we observe the Rabi oscillation when Γ_l is close to or below 1 kHz.

-
- [1] M. Born, E. Wolf, A. B. Bhatia, P. C. Clemmow, D. Gabor, A. R. Stokes, A. M. Taylor, P. A. Wayman, and W. L. Wilcock, *Principles of Optics: Electromagnetic Theory of Propagation, Interference and Diffraction of Light*, 7th ed. (Cambridge University Press, 1999).
- [2] C. R. Vidal, *Four-Wave Frequency Mixing in Gases* (Springer, 2005) Chap. 3.
- [3] B. Gary C, Effects of focusing on third-order nonlinear processes, *IEEE J. Quantum Electron.* **QE-11**, 287 (1975).
- [4] A. V. Smith and W. J. Alford, Practical guide for 7S resonant frequency mixing in mercury: generation of light in the 230-185- and 140-120-nm ranges, *J. Opt. Soc. Am. B* **4**, 1765 (1987).
- [5] A. V. Smith, W. J. Alford, and G. R. Hadley, Optimization of two-photon-resonant four-wave mixing: Application to 130.2-nm generation in mercury vapor, *J. Opt. Soc. Am. B* **5**, 1503 (1988).
- [6] C. Foot, *Atomic Physics*, Oxford Master Series in Physics (OUP Oxford, 2005).
- [7] O. Svelto, *Principles of Lasers* (Springer US, 2010).
- [8] A. V. Smith, G. R. Hadley, P. Esherick, and W. J. Alford, Efficient two-photon-resonant frequency conversion in mercury: the effects of amplified spontaneous emission, *Opt. Lett.* **12**, 708 (1987).
- [9] L. von der Wense, P. V. Bilous, B. Seiferle, S. Stellmer, J. Weitenberg, P. G. Thirolf, A. Pálffy, and G. Kazakov, The theory of direct laser excitation of nuclear transitions, *The European Physical Journal A* **56**, 1 (2020).